

INTERNATIONAL ATOMIC ENERGY AGENCY
UNITED NATIONS EDUCATIONAL, SCIENTIFIC AND CULTURAL ORGANIZATION



INTERNATIONAL CENTRE FOR THEORETICAL PHYSICS
34100 TRIESTE (ITALY) - P.O.B. 586 - MIRAMARE - STRADA COSTIERA 11 - TELEPHONES: 224281/2/3/4/5 6
CABLE: CENTRATOM - TELEX 460392-1

SMR/108-6

WORKSHOP ON NUCLEAR MODEL COMPUTER CODES

16 January - 3 February 1984

PARTICLE AND GAMMA RAY SPECTRA CALCULATIONS IN
STRUCTURAL MATERIAL

C. REFFO

E.N.E.A.
Via Mazzini 2
40126 Bologna
Italy

These are preliminary lecture notes, intended only for distribution to participants.
Missing or extra copies are available from Room 231.

PARTICLE AND GAMMA RAY SPECTRA CALCULATIONS IN STRUCTURAL MATERIAL

INVITED PAPER AT THE IAEA ADVISORY GROUP MEETING
ON STRUCTURAL MATERIAL

ABSTRACT: Models, codes, methodology and results have been reviewed for calculations of multiple particle and gamma ray emissions following neutron induced reactions from the resonance region to 25 MeV in some structural materials.

RIASSUNTO: Si presenta una panoramica di modelli, codici, metodi e risultati per calcoli di emissioni multiple in cascata di particelle e raggi gamma seguenti le reazioni indotte da neutroni nella zona risonante fino a 25 MeV in alcuni materiali strutturali.

PARTICLE AND γ RAY SPECTRA CALCULATIONS
IN STRUCTURAL MATERIAL

G. Reffo

ENEA, CRE "E. Clementel", Bologna, Italy

Abstract

The models, the methods and the results obtained in particle and γ ray spectra calculations for structural material are briefly outlined.

1. γ -ray emission.

1.1. The model and the code

The cascade model adopted has been illustrated in detail in ref. 1,2 and will be described here only briefly. Continuum bands are treated like discrete levels. For each band spin and parity dependent branching ratios are calculated allowing for the competition of E1, M1, E2 transition probabilities which are estimated according to Lorentz curve approximations to the respective giant resonances (GR) and using a Gilbert-Cameron⁽³⁾ (GC) level density formula, as parameterized in ref. 4.

A split GR model is used for E1 photon absorption, the Lorentzian parameters being taken from the systematics of ref. 4. Parameters for M1 and E2 Lorentz formulae are also taken from systematics⁽⁵⁾⁽⁶⁾.

The experimental branching ratios are used for discrete levels. Missing ones are estimated assuming single particle state transitions (with E1, M1 transitions dominating) for spherical nuclei and assuming collective transitions (with E2 transitions dominating) for collective nuclei.

These calculations were performed with our modular master code the IDA MODULAR SYSTEM⁽⁷⁾. It is capable of calculating integrated and differential cross sections for all reactions possible up to 50 MeV incident energies including most reaction mechanisms, whatever the projectile. As a particular option γ -ray cascades may be started at any step of the multiple cascading particle emission.

The main effort of the code is on organization. Cascade events are simultaneously ordered in as many different ways as there are purposes of the code i.e. according to a) stories with the same number of steps in the cascade (which allows for calculating cross sections of each γ -ray multiplicity and the corresponding partial spectra); b) cascades feeding levels a priori marked (for calculating excitation cross sections of marked levels, corresponding spectra and isomeric ratios, IR); c) emitted energy bands, where single-step contributions are lumped according to the respective γ -ray energies (for total γ -ray spectra calculations); d) initially a), b), c) are given for any J^π couple of the initial decaying level (this can be useful in several investigations e.g. either to isolate a), b), c) for given incident angular

momentum, 1, when the initial level is a compound nucleus one; or to estimate a), b), c), for a given $J\pi$ couple; etc.).

1.2. Rôle of relevant parameters

a) Optical model parameters

The optical model affects especially those calculations (like for IR determination) where the population probability of initial levels of given spin plays an important rôle and may be strongly influenced by the relative magnitude of strength functions (see ref. 2).

b) Giant resonance parameters (GRP)

GRP are involved only in the decay of continuum levels, where in most cases only one type (among E1, M1, E2) of transition dominates in each branching ratio. M1 or E2 transitions play their rôle when the other two types are forbidden. As a consequence, Lorentzian curve parameters do not greatly influence these calculations because they all tend to cancel out in the branching ratios, whenever γ -ray energies are smaller than the giant resonance peak energy.

For higher emitted γ -ray energies only peak energy (which is the best known) is expected to affect calculations.

c) Level density parameters

The result of γ -ray cascade calculations greatly

depends on the level density and level schemes adopted.

In spite of the encouraging success of recent investigations (especially BCS), the corresponding model parametrizations do not yet offer the same confidence level as the model and the systematics⁽⁴⁾ here adopted. The validity of this approach has been recently discussed in ref. 8.

The effect of the spin distribution of level density was tested on ^{241}Am calculations⁽¹⁾, by reduction of the spin cut off factor by a factor of 2. This produced only slight effects with a shift of the spectrum toward the soft part. In addition an increase in IR of 5% was observed.

As far as the low energy region is concerned large difficulties arise where discrete level informations is missing (like energy levels, their quantum characteristics or branching ratios).

In the case of the spectrum for gold we have investigated the impact of the following assumptions: (i) all known levels (28, at all, up to .571 MeV) are neglected, and replaced by the level density treatment; (ii) all discrete levels have been included, but experimental branching ratios are replaced by theoretical estimates according to sec. II.

The resulting spectra, dashed and dotted histograms, respectively, are given in fig. 1 together with the result of the standard calculation, full line.

As can be observed from the figure, hypothesis i) is much too crude and introduced severe changes in the energy

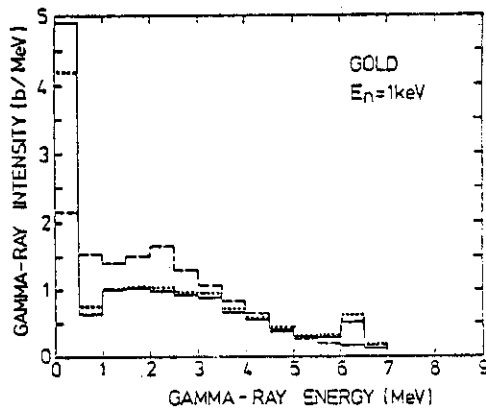


Fig. 1

trend of the spectrum. On the contrary hypothesis ii) does not appreciably influence the final result.

The influence of the discrete level scheme on isomeric ratio calculations (here $= \sigma_g(n, \gamma) / \sigma(n, \gamma)$) has been investigated in ^{241}Am (2) at 30 KeV, where a value $\text{IR} = .75$ is obtained from standard calculations.

Skipping half of the discrete levels we got $\text{IR} = .69$, while, by skipping the complete level scheme we obtained $\text{IR} = .5$.

No significant difference was observed through replacing E2 collective transition probabilities by E1, M1 single particle transition probabilities.

7

d) Effect of width fluctuations

It was assumed that width fluctuations effects influence only the primary γ -ray spectrum. An investigation of the width fluctuation correction on the primary γ -ray spectrum leads to the conclusion that (exception made for very weak transitions, which are strongly enhanced) single transition probabilities are affected by correction factors very close to that of the corresponding integral cross section.

Thus the whole primary spectrum is uniformly shifted by width fluctuation correction factor.

e) Energy dependence of γ -ray intensities

Essentially one has three types of energy dependences for E1 transitions:

- i) E_γ^3 , according to Blatt-Weisskopf single particle transitions.
- ii) E_γ^5 , according to Axel.
- iii) E_γ^7 , according to Dover et al. (9), Arenhovel et al. (10), Gardner et al. (11).

Recently McCullagh et al. (12) found experimental evidence for an $E_\gamma^{5.5}$ energy dependence, while Raman (13) verified that the validity of the Brink-Axel hypothesis has only a few exceptions.

The impact of the above three assumptions has been investigated in the total spectrum calculation of gold where measurements are available from ref. (14). To this end fig. 20 of ref. (11) is here reproduced as fig. (2), where we have

8

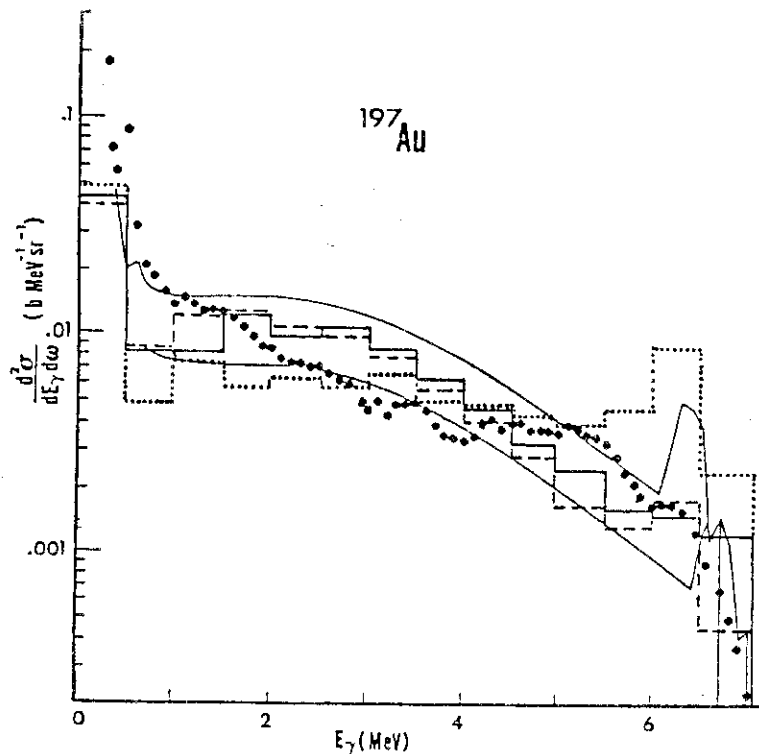


Fig. 2

plotted, for comparison, our results (hystograms).

The data in fig. 2 correspond to the following incident neutron energies: the experimental ones are measured in the interval .2÷6. MeV, the two full line curves have been calculated⁽¹¹⁾ at .2 and .6 MeV, respectively while the hystograms at .4 MeV. (It should be noted that the spread

of neutron energies, ΔE≈.4 MeV, may affect the comparison of present calculations especially in the last hystogram step).

One observes that the spectrum from our E_Y^5 -calculation, full line hystogram, well agrees with the Gardner et al⁽¹¹⁾ spectrum, except for the hard part. This seems in contradiction with the wrong trend of the E_Y^7 -calculation (dotted hystogram) which clearly favours the hard tail against the soft one, as expected.

Except for the hard tail of the spectrum, no remarkable difference is observed between E_Y^5 - and E_Y^3 - calculations (dashed hystogram).

On the whole, one may conclude on the better results of the E_Y^5 -law, in agreement with the mentioned experimental investigations of refs (12) and (13).

As far as M1 and E2 transitions are concerned, there is not sufficient information for a more than tentative treatment.

Finally, it must be noted that only the Brink-Axel approach allows for absolute calculations of $\Gamma_Y(B_n, J, \Pi)$, as shown in refs. (15), (16), provided correct parametrization is adopted for both the level density and Lorentz-curve.

1.3. γ -decay calculations in structural material. The rôle of E1 and M1 transitions and of Valence mechanism

In the literature, in general, one assumes that E1 tran-

sitions dominate the γ -ray decay of composite systems. Here we have selected some structural materials of interest in reactor technology, where the necessity of accounting also for M1 transitions is shown by means of detailed model calculations. The rôle of Valence reaction mechanism is also illustrated by few examples.

We have estimated the E1 and M1 contributions to the total and partial average radiative widths and to the average total γ -ray spectra following s-, p-, d-wave neutron capture in the resonance region of $^{58,60}\text{Ni}$ and ^{56}Fe .

The adopted parameterization is shown in table 1. the level schemes adopted were taken from ref. 17, while missing γ -ray branching ratios of discrete levels were estimated by means of the well known Weisskopf transitions probabilities. Level density parameterization was done according to ref. 3.

table 1

Summary of adopted parameters for the calculation of level densities and radiative widths.

Model param.	a	U_x	T	β	σ^2	D _{OBS}	E ₁	Γ_1	σ_1	E ₂	Γ_2	σ_2	E _{M1}	Γ_{M1}	σ_{M1}
Isotope	MeV ⁻¹	MeV	MeV			keV	MeV	MeV	mb	MeV	MeV	mb	MeV	MeV	mb
^{58}Ni	7.32	8.2	1.31	.17	7.3	14.	16.0	3.7	53	18.6	5.1	75	11.8	2.36	10.6
^{60}Ni	8.4	7.3	1.2	.17	4.5	14.	16.0	3.7	55	18.4	5.1	78	11.7	2.34	11.0
^{56}Fe	8.52	6.9	1.14	-.25	5.1	19.	17.5	4.8	77	21.4	4.95	39	12.0	2.4	10.3

M1 transition probabilities were estimated in terms of a giant resonance model the parameterization of which was determined (see table 1) by normalization of the strength to the systematics of ref. 6.

Calculated average total E1 and M1 radiative widths are shown in table 2 for the various J^π quantum numbers involved in the respective resonance regions of $^{58,60}\text{Ni}$ and ^{56}Fe . The effective number of degrees of freedom of the lumped χ^2 distributions are also given in order to quantify the size of the statistical fluctuations characterizing the various calculated as well as measured radiative widths.

table 2

Calculated average E1 and M1 contributions to the total radiative width for s-, p- and d- wave resonances compared to results evaluated from experimental data.

Isotope	l	J^π	$\bar{\Gamma}_\gamma$ (E1)	ν_{eff}	$\bar{\Gamma}_\gamma$ (M1)	ν_{eff}	$\bar{\Gamma}_\gamma^{\text{EXP}}$	Ref.	$\nu_{\text{eff}}^{\text{EXP}}$
^{58}Ni	0	$\frac{1}{2}^+$	2200 \pm 883	12	113 \pm 38	17			
	1	$\frac{1}{2}^-$	766 \pm 244	20	456 \pm 234	8			
		$\frac{3}{2}^-$	726 \pm 230	20	380 \pm 153	12			
	2	$\frac{3}{2}^+$	1823 \pm 602	18	106 \pm 36	18			
		$\frac{5}{2}^+$	1387 \pm 444	20	97 \pm 32	18			

table 2 continues

isotope	J ^π	$\Gamma_Y(E1)$	ν_{eff}	$\Gamma_Y(M1)$	ν_{eff}	Γ_Y^{EXP}	Ref.	ν_{eff}^{EXP}
⁶⁰ Ni	0 $\frac{1}{2}^+$	1050 \pm 420	12	59 \pm 21	16	1300 \pm 70	[18]	
	1 $\frac{1}{2}^-$	443 \pm 148	18	208 \pm 98	9	1200	[18]	
	$\frac{3}{2}^-$	401 \pm 132	19	190 \pm 69	15			
	2 $\frac{3}{2}^+$	1109 \pm 353	20	53 \pm 18	17			
	$\frac{5}{2}^+$	896 \pm 268	22	45 \pm 15	18			
⁵⁶ Fe	0 $\frac{1}{2}^+$	1070 \pm 428	11	34 \pm 12	15	850 \pm 410	[19]	9.6
	1 $\frac{1}{2}^-$	246 \pm 87	16	203 \pm 97	9	500 \pm 180	[19]	17.1
	$\frac{3}{2}^-$	231 \pm 75	19	162 \pm 64	13			
	2 $\frac{3}{2}^+$	900 \pm 313	17	32 \pm 11	18	730 \pm 250	[19]	18.5
	$\frac{5}{2}^+$	652 \pm 224	17	25 \pm 8	18			

On the whole a good agreement, within statistical fluctuations, is obtained between the calculated and experimental quantities given in table 2.

In table 3 we quote the calculations for one well known s-wave resonance E_λ for each isotope considered. For each resonance the total as well as the partial radiative width for the transitions to the first two excited level of energy E_μ are given. Γ_Y^0 is the reduced neutron width.

13

table 3

Calculated partial and total gamma widths for s-wave resonances. Quoted uncertainties are the standard deviation of the respective statistical χ^2 distributions.

isotope	E_λ (keV)	E_μ (keV)	Γ_λ^0 (eV)	$\Gamma_Y^{C.N.}$ (meV)	Γ_Y^{VAL} (meV)	Γ_Y^{TOT} (meV)	Γ_Y^{EXP} (meV)	Ref.
⁵⁸ Ni	15.4		9.19	2200 \pm 40%	62	1745 \pm 50%	1530 \pm 7%	[20]
		0		340	35	150	124 \pm 17	[21]
		465		305	18	176	110 \pm 19	[21]
⁶⁰ Ni	12.3		23.98	1050 \pm 40%	127	1670 \pm 50%	2920 \pm 7%	[20]
		0		178	60	444	514 \pm 72	[21]
		283		150	57	380	289 \pm 46	[21]
⁵⁶ Fe	27.7		8.72	1070 \pm 40%	145	650 \pm 50%	1090 \pm 5%	[10]
		0		183	12	103	145 \pm 25	[21]
		14		182	71	26	35 \pm 13	[21]

For the valence mechanism we found a negligible M1 contribution, but an E1 contribution which seems to affect rather significantly the total radiative width Γ_Y^{TOT} , provided an interference term is accounted for

$$(\Gamma_{Y\lambda\mu}^{TOT})^{1/2} = (\Gamma_{Y\lambda\mu}^{CN})^{1/2} + (\Gamma_{Y\lambda\mu}^{VAL})^{1/2}$$

The valence model adopted, namely is the one by Lane-Mughabghab (22) according to the specifications in ref. 23.

Percentual error quoted with calculated quantities are

14

the standard deviations of the corresponding χ^2 lumped distribution.

$$S.D. = \sqrt{2/\nu} \langle \Gamma \rangle$$

ν being the effective number of degrees of freedom.

As an example, in fig. 3, the average compound nucleus total γ -ray spectrum (full line) and separately only the E1 contribution (dashed line) are given for ^{58}Ni in the resonance region.

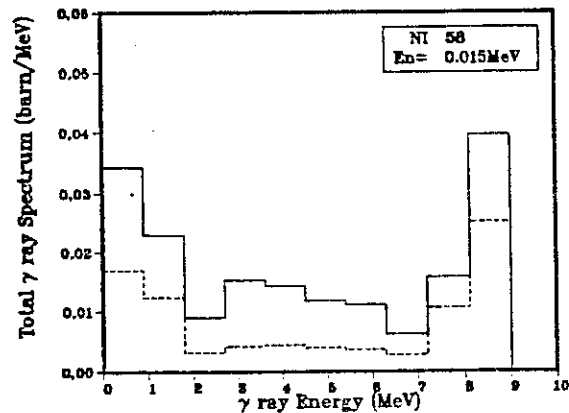


Fig. 3

In fig. 4 again for the same case, the different shapes are shown of the s- (full line) and p-wave spectra ($J=1/2$, $=3/2$ dotted and dashed line, respectively). Due to the parity selection rules of γ -ray transitions the s- and d-spectra are dominated by E1 transitions, while the p-spectrum by M1 ones.

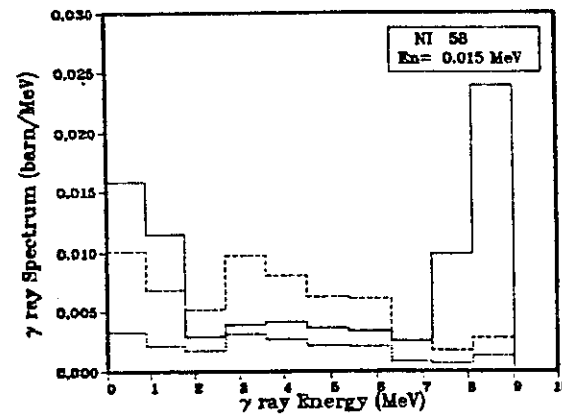


Fig. 4

1.4. Importance of valence mechanism in neutron capture

Because valence mechanism mostly affect the resonance region, the effects of valence mechanism in neutron capture are to be considered also dealing with average cross sections.

In order to illustrate the subject, the case of ^{86}Kr has been chosen because, differently from the structural materials, for this isotope one has the availability of recent measurements for the average cross section of neutrons with maxwellian energy distributions peaked at 30 KeV:

$$\langle \sigma_{n,\gamma} \rangle = (5.6 \pm 0.7) \text{ mb}^{(24)}; \quad \langle \sigma_{n,\gamma} \rangle = (4.6 \pm 0.7) \text{ mb}^{(25)};$$

$$\langle \sigma_{n,\gamma} \rangle = (4.8 \pm 1.2) \text{ mb}^{(26)}.$$

In addition ^{86}Kr neutron resonance characteristics are also available from ref. 26.

All these experimental information makes possible the

study of ^{86}Kr KeV neutron capture to test the validity and the role played by compound nucleus and valence capture mechanisms.

In Table 4 a selection, out of ref. 26, is reported for the ^{86}Kr neutron resonances of known characteristics.

Table 4. Experimental and calculated neutron resonance characteristics in ^{86}Kr .

E_n	J^π	$g\Gamma_n$	$\text{EXP } \Gamma_Y^{J\pi}$	$\langle \text{EXP } \Gamma_Y^J \rangle_L$	$\langle \text{STAT } \Gamma_Y^J \rangle_L \pm \text{S.D.}^v$ M1, E1	$\text{VAL } \Gamma_Y^J$ M1, E1	$\text{TOT } \Gamma_Y^{J\pi}$
36.93	$\frac{1}{2}^+$	53	300 \pm 80	250 \pm 80	200 \pm 80 ¹⁰	40	240 \pm 80
42.91	$\frac{1}{2}^-$	125	390 \pm 100	360 \pm 100	340 \pm 200 ⁶	20	360 \pm 200
49.64	$\frac{1}{2}^+$	42	200 \pm 60	250 \pm 80	200 \pm 80 ¹⁰	15	215 \pm 80
54.37	$\frac{3}{2}^-$	402	550 \pm 150	550 \pm 150	390 \pm 200 ⁸	210	600 \pm 200
28.86	$\frac{1}{2}^-$	95	330 \pm 120	360 \pm 120	340 \pm 200 ⁶	15	355 \pm 200

In the columns from left to right one has the resonance energies E_n ; the quantum characteristics J^π ; the neutron widths, $g\Gamma_n$; total measured radiative widths $\text{EXP } \Gamma_Y^{J\pi}$; average s- and p-wave total experimental radiative widths per spin state $\langle \text{EXP } \Gamma_Y^J \rangle$; average s- and p-wave total radiative widths per spin state $\langle \text{STAT } \Gamma_Y^J \rangle_L \pm \text{S.D.}^v$ calculated in terms of Brink-Axel model for compound nucleus radiative decay⁽⁴⁾, inclusive

of M1 and E1 transitions, S.D. being the standard deviation of the lumped χ^2 distribution of all partial widths and v the inherent number of degrees of freedom; total valence contribution as a sum of E1 and M1 contributions $\text{VAL } \Gamma_Y^J$; total calculated radiative width $\text{TOT } \Gamma_Y^J$ as a sum of valence and compound nucleus contribution (both E1 and M1 transitions included), without interference effect.

In order to determine the expectation value of the n, γ cross section at 30 KeV the usual Hauser-Feshbach theory with width fluctuation correction has been used. This was parameterized using the mean spacing of s-wave resonances, $D_{\text{OBS}} = (40 \pm 14)$ KeV, deduced from the complete set of data of ref. 26 and normalizing the calculated $\Gamma_Y^{J\pi}$ to the corresponding average values in column 5 (see Table 4). It is important to note here that the adopted values for D_{OBS} is in perfect agreement with the local systematics of the level density parameter "a" deduced for the families of Kr, Se, Br isotopes.

So far the value which can be obtained in terms of statistical model is $\langle \sigma_{n, \gamma} (30 \text{ KeV}) \rangle = 20 \text{ mb}$, 4 times greater than experimental ones.

The idea to overcome the discrepancy found by assuming a valence contribution comes from the large value $\rho = .94$ of the correlation coefficient between the measured values for Γ_n and Γ_γ . In particular, from the comparison of experimental and calculated quantities in table 4 one can

see that the large Γ_Y^{EXP} observed at 54.37 KeV comes from the large E1 valence transitions correlated to the large Γ_n values. Differently, the fluctuations observed for the Γ_Y^{EXP} of the other quoted resonances mostly are denominated by statistical fluctuations according to the very low number of degrees of freedom characterizing the lumped width distribution in all cases, see Column 6. The very good overall agreement between columns 4 and 7 suggests that the appropriate average $\langle \Gamma_Y^{\text{J}\Pi} \rangle$ values to be used in capture calculations are just the Brink-Axel model ones⁽⁴⁾ quoted in column 6, without any normalization to the experimental ones.

One finds that at 30 KeV the valence contribution to neutron capture is negligible because it affects only a few channels feeding the lower lying levels in ^{87}Kr , out of the bulk of all other innumerable statistical channels.

On the contrary the compound nucleus contribution dominates and is so found to be $\langle \sigma_{n,\gamma} (30 \text{ KeV}) \rangle = (8 \pm 2.7) \text{ mb}$, the quoted uncertainty being due to that of D_{OBS} , according to error propagation.

2. NEUTRON EMISSIONS

2.1. The models and the code

Careful studies of the neutron induced reactions at 14-15 MeV on structural material are requested as a part

of fusion neutronic. A few model calculations on ^{56}Fe , ^{93}Nb , ^{59}Co performed in this contest, are here presented. The rôle of equilibrium and preequilibrium emissions and the limits and validity of the model are illustrated.

Our results are obtained improving the unified exciton model extensively described in ref. 27,28 by the introduction of the principle of conservation of total angular momentum. This, also, implied the use of a suitable particle-hole spin dependent level density.

Since one can show that the master equations as well as the methods of ref. (27), still apply, then the new occupation probability $q^{\text{J}\Pi}(n, \Omega, t)$ of the composite nucleus state (n, Ω, J, Π) (where n and Ω are the exciton number and the direction of the projectile inside the nucleus, and J and Π denote the total angular momentum and parity of the composite nucleus at time t) can be expressed as a Legendre polynomial series:

$$q^{\text{J}\Pi}(n, \Omega, t) = \sum_{\ell} \eta_{\ell}^{\text{J}\Pi}(n, t) P_{\ell}(\Omega) .$$

The time-integrated master equation is then given by:

$$\begin{aligned} - \eta_{\ell}^{\text{OJ}\Pi}(n) &= \nu_{\ell} \lambda^{+}(n-2) Z_{\ell}^{\text{J}\Pi}(n-2) + \nu_{\ell} \lambda^{-}(n+2) Z_{\ell}^{\text{J}\Pi}(n+2) \\ &- [W^{\text{J}\Pi}(n) + \lambda^{+}(n) + \lambda^{-}(n) + (1-\nu_{\ell}) \lambda^{\circ}(n)] Z_{\ell}^{\text{J}\Pi}(n) \end{aligned}$$

the λ^{+} , λ^{-} and λ° are the intranuclear transition rates and

w is the total emission rate.

Here we assume J-independent transition rates, but this generally adapted assumption must be reconsidered.

The ρ_l are the eigenvalues of the intranuclear scattering Kernel, $\eta_l^0(n)$ refers to the Legendre coefficients of the initial (t=0) occupation probability, and $z_l^{J\Pi}(n)$ are the Legendre coefficients of the mean lifetime of the nuclear state (n, Ω , J, Π).

The double differential cross section including equilibrium and preequilibrium emission is

$$\frac{d^2\sigma(a,b)}{d\epsilon d\Omega} = \frac{\pi^2}{(2s_a+1)(2I+1)} \sum_{J\Pi} T_{l_a j_a}^{J\Pi}(e_a) \sum_n W_b^{J\Pi}(n, \Omega) \tau^{J\Pi}(n, \Omega)$$

where $T_{l_a j_a}^{J\Pi}(e_a)$ are the optical model transmission coefficients J and I denote the composite and target nucleus total angular momentum respectively, l_a , s_a and j_a are the orbital angular momentum, spin and total angular momentum of incident particle, $W_b^{J\Pi}(n, \Omega)$ is the probability of emission of particle b with energy ϵ_b from the exciton state (E, n, J, Π) $\tau^{J\Pi}(n, \Omega)$ is the mean lifetime of this state and n run over all possible exciton configurations.

A particular mention must be devoted to the J dependent p-h level density involved in the model.

Namely a Williams' formula⁽²⁹⁾ was adopted, normalized to reproduce the total level density observed according to ref. 30.

Following ref. (31) the distribution of the p-h states on the spin projection M was assumed to be of a Gaussian type. An exciton dependent spin cut off was found⁽³¹⁾, $\sigma_n =$

$= .28n A^{2/3}$ valid through the whole periodic table.

Calculations are performed with the modular master Code IDA above mentioned⁽⁷⁾. Spherical optical model transmission coefficients are used. On option, self consistent calculations in generalized optical model approximation may also be requested. Up to four subsequent particle emissions are allowed followed by a γ -ray cascade of maximum multiplicity 7. Integral or double differential cross sections can be calculated for any single emission process, as well as total spectra and angular distribution for any given emission type. The unified model⁽²⁷⁾ with conservation of total angular momentum is used for the description both of equilibrium and pre-equilibrium emissions.

The master code consists of modules, one for each step of the calculation procedure, from neutron resonance statistical analysis and from optical model parameter automatic search to the more sophisticated calculations, like isomeric cross sections in a multiple particle emission reaction and to the data management and graphical display.

The whole calculation is completely automatized. Where no particular check is necessary against available experimental data, thanks to a shared nuclear data library, only Z, A energy and projectile are sufficient to get the complete information allowed by the system.

Calculations were performed using the neutron optical model of ref. 32.

In the figs. 5-10, the contribution of the unified model

to equilibrium and preequilibrium emissions (namely the primary emissions) and of all the energetically possible secondary equilibrium emissions according to Hauser-Feshbach theory are the dashed and dotted histograms respectively. The sum of the two contributions gives the total neutron emission spectrum, full line histogram.

In fig. 5 the calculated total spectrum is compared to an average spectrum, full line curve, obtained averaging over all experimental data available. Here the model appears to overestimate the hard tail of the spectrum, where lower exciton state emissions are expected to dominate.

In figs. 5 to 10 the total spectrum at different angles is given, the dots representing the measurements of ref. 33. In these figures one observes an agreement between the calculated and experimental spectra which is very good at backward angles while worsening at forward angles, again where the lower exciton contributions are involved.

The consistent answer obtained from the comparison of total and partial spectra, seems to suggest a wrong exciton dependence of the adopted p-h level density. (Really all statistical assumptions underlying Williams' formula breakdown at low exciton numbers, where more appropriately combinatorial calculations should be used).

In fig. 11 we show the results of the angular distribution of the neutrons with energy $E = 2-3$ MeV (where equilibrium emissions dominate) and of the neutrons with energy $E = 8-9$ MeV (where preequilibrium emissions dominate).

Here a level density from combinatorial calculations has been used.

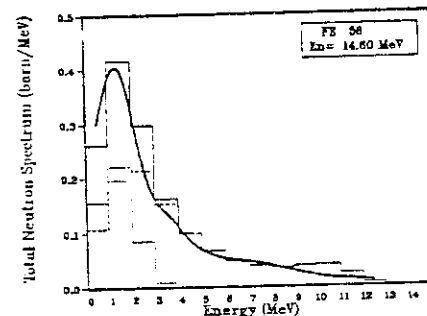


Fig. 5

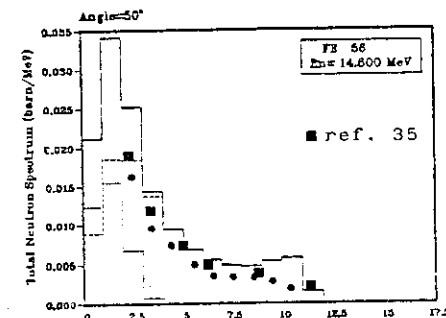


Fig. 6

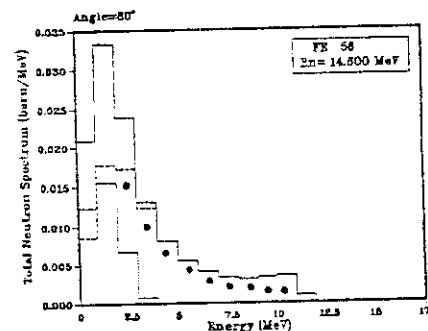


Fig. 7

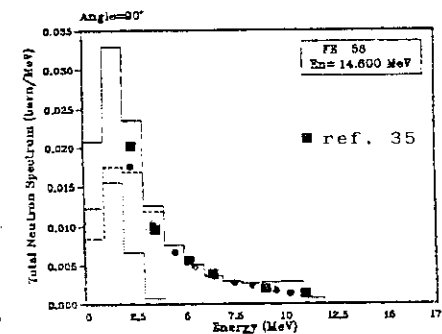


Fig. 8

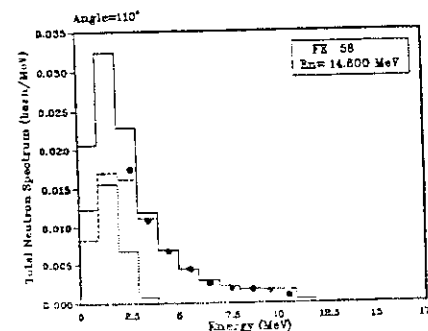


Fig. 9

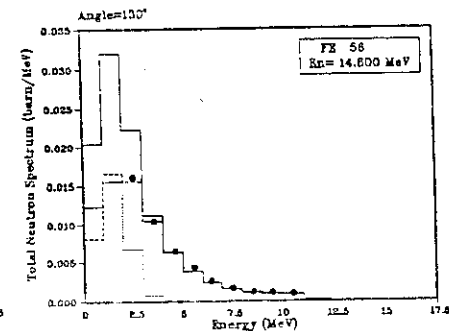


Fig. 10

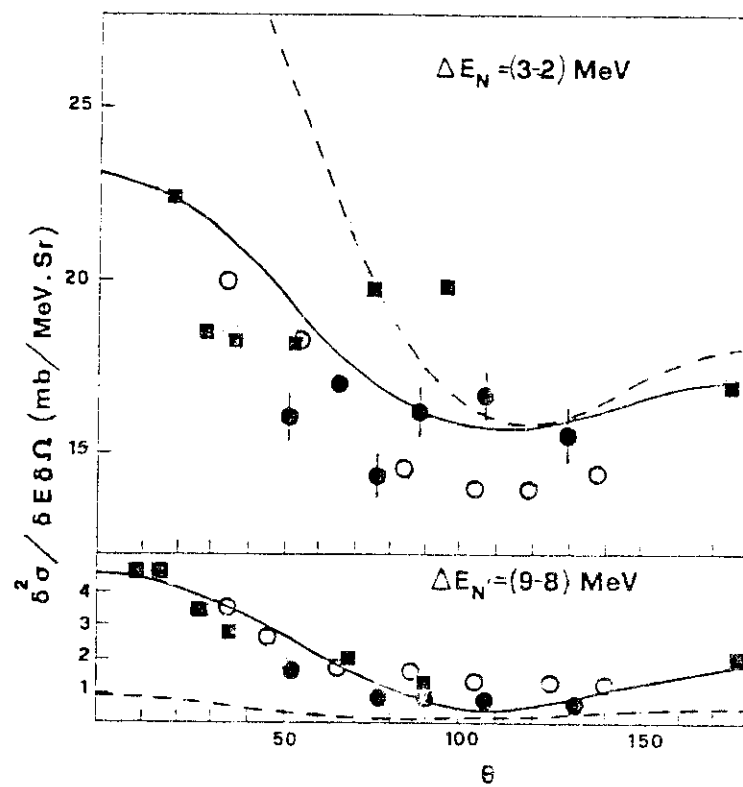
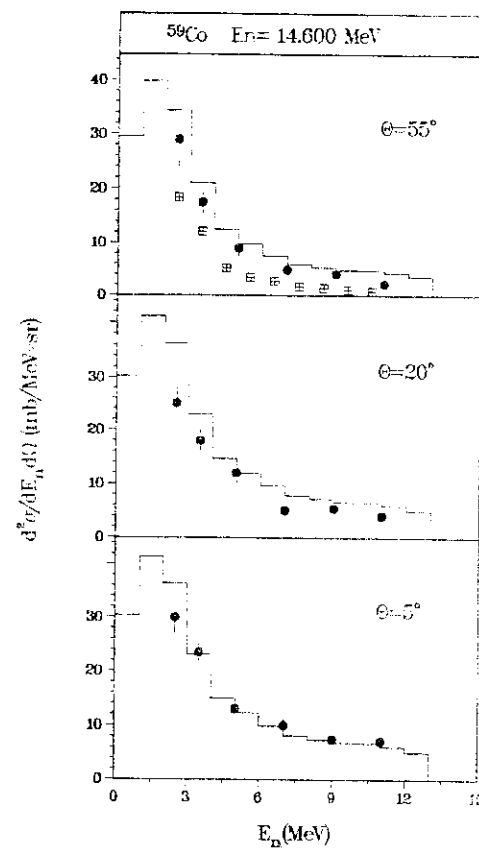


Fig. 11



□ = Zrk-27, INDC(gdr)-2/L
● = Soviet J. N.P.34(299)(1981)

Fig. 12

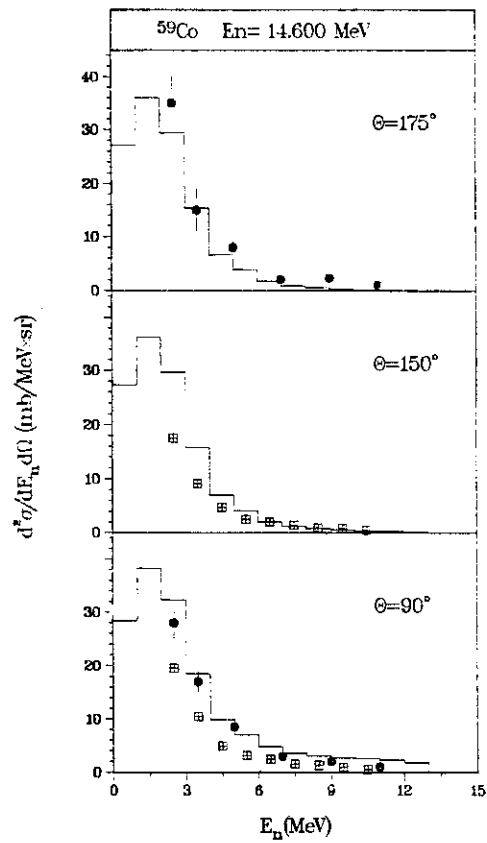


Fig. 13

□ = Zfk-277 IND(gdr)-2/L
 • = SovietJ. N.P.34(299)(1981)

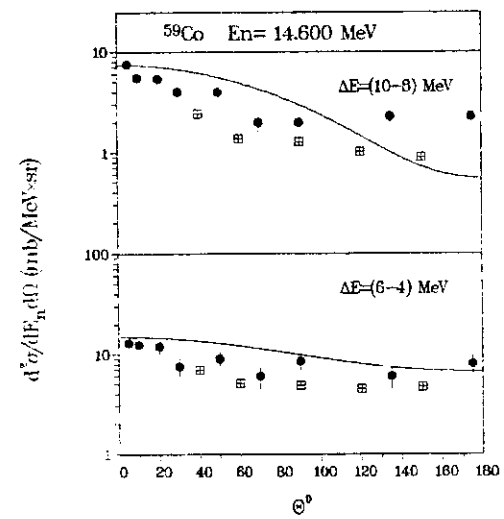


Fig. 14

□ = Zfk-277 IND(gdr)-2/L
 • = SovietJ. N.P.34(299)(1981)

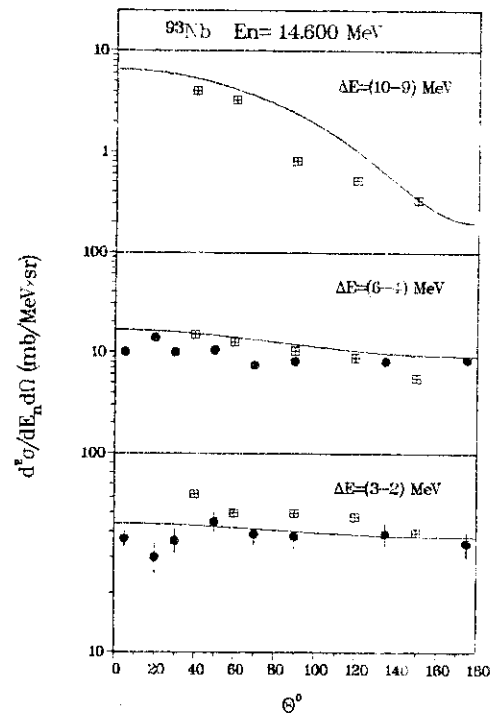


Fig. 15

□ = Zfk-277 INDC(gdr)-2/L
 ● = SovietJ. N.P.34(299)(1981)

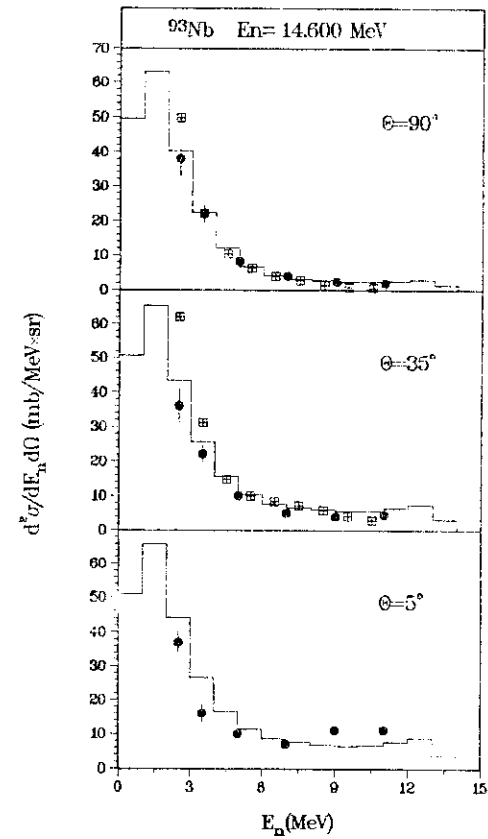


Fig. 16

□ = Zfk-277 INDC(gdr)-2/L
 ● = SovietJ. N.P.34(299)(1981)

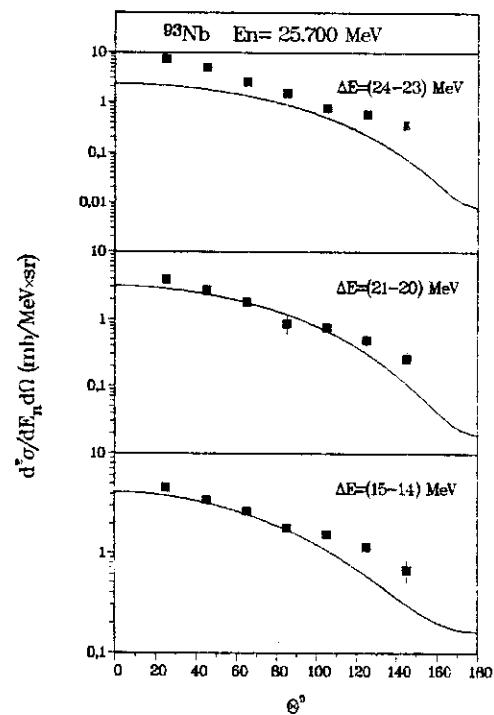
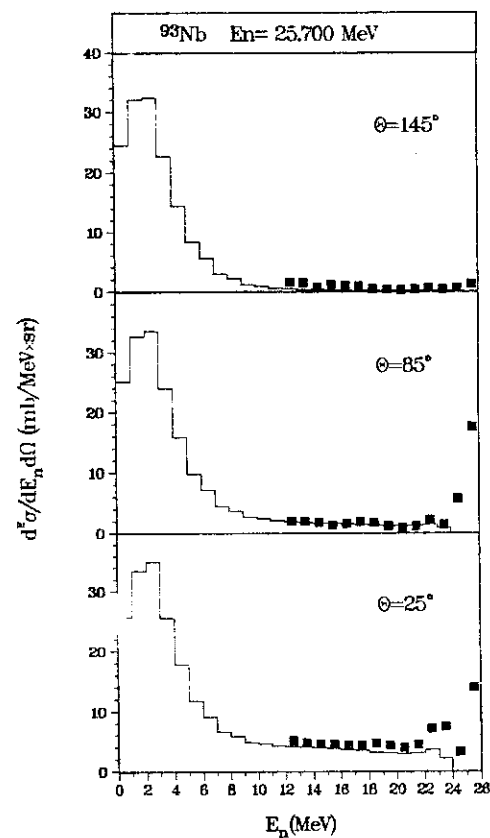


Fig. 17

■ = Marcikowski N.S.E. 83,13 (1983)



■ = Marcikowski N.S.E. 83,13 (1983)

Fig. 18

Dots and open circles are the measurements of ref. 31 and ref. 34 respectively. In the lower part of fig.11, to be consistent with previous results, one would expect that the spectrum calculated at forward angles be higher than the corresponding experimental one. This, however, is not the case for open circle data, neither for the data of ref. 31 (squares). This fact and the spread of points in the upper part of the figure rise questions on a possible rôle of experimental uncertainties in the discrepancies found. In figs. 12 to 14 we show the results of the calculations for ^{59}Co at 14.5 MeV obtained using the input ⁽³⁶⁾ fixed in the frame of the international intercomparison of codes for compound nucleus calculations, sponsored by the NEA DATA BANK. In figs. 15 and 16 we show the results of the calculations for ^{93}Nb at 14.5 MeV obtained using the input ⁽³⁷⁾ fixed in the frame of the international intercomparison of codes for pre-equilibrium calculations, sponsored by NEA DATA BANK.

In figs. 17 and 18 the results of calculations in ^{93}Nb at 25.6 MeV are also shown, using the same input.

From all the cases here illustrated one can see that calculations compare to experimental data substantially good and always the same way. At 14.5 MeV we repeated the calculations after replacement of the free nucleon scattering assumed in ref. 27 by the scattering of nucleons bound in a square well and after introduction of the refraction term of nucleons beams at the nuclear surfaces.

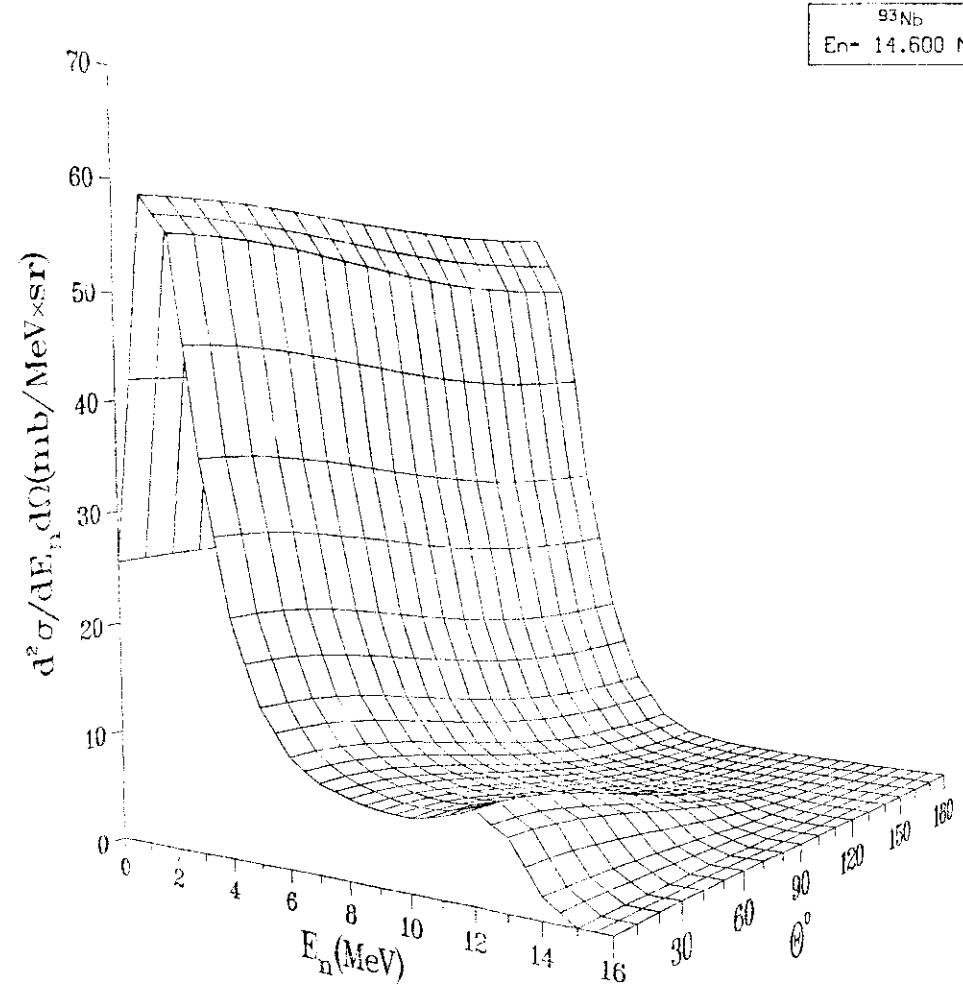


Fig. 19

The calculations with inclusion of the latter refinements did not show any substantial improvement with respect to the previous one. In particular the two effects considered showed evidence for a reciprocal cancellation.

In fig. 19 one can see very well the physical features of the two reaction mechanisms involved. Namely at low emitted neutron energies one has the bulk of the spectrum with a symmetric angular distribution characteristic of equilibrium emissions (dominant process) while at high emitted neutron energies one finds forward peaked emissions characteristic of a dominant preequilibrium process.

Conclusions

Spectra and IP calculations are valuable in view of the need for them in a number of applications and of the measurement difficulty.

Recently, spectra calculations offered appreciable help in correcting systematic errors of relative neutron radiative capture measurements made with Moxon-Rae detectors ^{(1), (2), (5)}.

A number of recent experiments proves the validity of basic assumptions adopted for the energy dependence of γ -ray intensities.

A weak point of these calculations remains however the determination of reliable level schemes and inherent γ -ray branchings when these are not measured. In fact, the consi-

derable theoretical efforts in this direction proved very useful in understanding nuclear structure, but cannot yet replace all cases where experimental information is missing. A possible improvement of present calculations may be obtained by the introduction of considerations of rotational bands in order to fill the gaps in level schemes and introducing K-selection rules in the γ -ray transitions.

In view of these difficulties, stress should be laid on the need for experts to provide cross section evaluators with appropriate level schemes, at least for the cases of recognized interest.

From the model calculations illustrated one can realize that M1 contributions cannot be neglected in the theoretical estimate of any of the quantities here discussed, where a nuclear structure which favours M1 transitions (via the play of J π selection rules) couples to M1 transition strength comparable to that of E1 transitions.

From the example illustrated, one may conclude that even if valence mechanism do not contribute appreciably to neutron capture cross section nevertheless, in specific nuclei, it may be of great help in explaining apparently ambiguous situations and in determining the appropriate model parameterization.

The case considered also gives additional evidence for the validity of the adopted models for radiative decay of compound nucleus and capture cross section calculations.

For the particle emissions at 14.5 Mev, one has to say that a considerably better result is obtained with the improvements illustrated and introduced into the previous version⁽²⁷⁾ of the unified exciton model. This is mainly achieved because

- i) the unified model allows for a consistent treatment of both equilibrium and pre-equilibrium contributions.
- ii) Introduction of the principle of conservation of total angular momentum allows for a proper weighting of all reaction channels, according to the spin distribution of the p-h level density.
(Out of curiosity, in fig. 9 the results of calculations are shown too, dashed curve, with no angular momentum conservation).
- iii) Introduction of the appropriate distribution of p-h levels, according to spin, allowed for the most meaningful extension mentioned in ii) above.

From the sample calculations illustrated some conclusions may be derived.

It appears very likely that the moderate discrepancies observed are due more to the very rough total level density adopted (especially for lower excitation numbers), than to conceptual inadequacy of the model.

In particular to achieve the best results, the necessity appears of a consistent treatment of equilibrium and pre-equilibrium

contributions like the unified model can provide us with.

One may say that the model, even as it is, is reliable in giving an overall picture of total and partial emission spectra as well as of angular distributions. In addition, because no free parameters were used, these results may be regarded as a model test proving a wide prediction capability valid also if no experimental information is available.

In general, one may conclude that considerable results have been achieved in the calculation of total and partial particle and γ -ray emission cross sections. Namely calculations are now possible even if no experimental information is available, because the degree of accuracy is, more or less known, and may be estimated pretty close to usual experimental uncertainties for the quantities inherent to γ -ray emission and, at worse, <100% for particle spectra emission calculations in the higher energy tails.

REFERENCES

- (1) Wisshak K., Wicknehauser J., Käppeler F., Reffo G., Fabbri F., Nucl.Sc.Eng. 81 (1982) 396.
- (2) Reffo G., Fabbri F., Wisshak K., Käppeler F., Nucl. Sc. Eng. 80 (1982) 630.
- (3) Gilbert A., Cameron A.G.W., Can.Journ. of Phys., 43 (1965) 1446.
- (4) Reffo G., IAEA Report SMR-43 (1980) p.205. Lecture held at the "Winter Course on Nuclear Physics and Reactors" at ITCP Trieste, 17 Jan. - 10 Mar. 1978.
- (5) Reffo G., Fabbri F., Wisshak K., Käppeler F., Nucl. Sc.Eng. 23 (1983) 401.
- (6) KOPECKI J., Proc. of the 4th (n.) Int. Symp., Grenoble 7-11 Sept. 1981, pag. 23. Inst. of Phys. Conf. Series n. 62. Bristol and London.
- (7) Reffo G., Fabbri F., IDA modular System Not torino 13 E.
- (8) Reffo G., "Limits and Validity of the phenomenological Gilbert-cameron level density approach, Invited paper at the IAEA advisory group meeting on "Basic and applied Problems of Nuclear Level Densities". Brookhaven Not. Lab. (USA) April 11-15 1983.
- (9) Dover C.B., LEMMER R.H., HALME F.J.W., Ann. Phys. (N.Y.) 70 (1972) 458.
- (10) Arenhovel H., Grainer W., Danos M., Phys. Rev. 157 (1967) 109.
- (11) Gardner D.G., Gardner M.A., Dietrich F.S., Report UCID-18759, August 7, 1980 and in Nuclear Cross Sections for Technology, edited by J.L. Fowler, C.H. Johnson and C.D. Bownman (NBS (Special Publication No. 594), Washington D.C. 1980).
- (12) McCullagh C.M., Stelts M.L., Chrien R.F., Phys. Rev. 23, 1394 (1981).
- (13) Raman S., invited paper at IV Int. Symposium on Neutron Capture Gamma-Ray Spectroscopy and Related Topics, Sept. 7-11, 1981, Grenoble.
- (14) Morgan G., Newman E., Report ORNL-TM-4973, August 1975.
- (15) Benzi V., Reffo G., Vaccari M., Contributed paper to the IAEA "Fission Product Nuclear Data Meeting", Bologna 26-30 Nov. 1973. Report IAEA 169, pag. 123 (1974).
- (17) Lederer C.M. and Shirley V.S., Tables of isotopes, 7th ed., John Wiley & Sons, Inc. New York (1978).
- (18) Perey C.M., Harvey J.A., Macklin R.L., Winters R.R. and Perey F.G., "Neutron transmission and capture measurements and analysis of ⁶⁰Ni from 1 to KeV, ORNL-5893, ENDF- 330, Oak Ridge National Laboratory, November 1982.
- (19) Corvi F., Brusegan A., Buyl R., Rohr G., Shelley R. and Van der Veen T., Proc. Int. Conf. on Nuclear Data for Science and Technology, Antwerp 6-10 September 1982.
- (20) Wisshak K., Käppeler F., Reffo G., Fabbri F., Neutron Capture in s-wave resonances of ⁵⁶Fe, ⁵⁸Ni and ⁶⁰Ni, KfK report 3516, July 1983.
- (21) Beer H., Spencer R.R. and Käppeler F., Zeitschrift für Physik A 284, 173 (1978).
- (22) Lane A.M., Mughabghab S.F., Phys. Rev. C 10 (1974), 412.
- (23) Mengoni A., Reffo G., International Conf. on Nuclear Data for Science and Technology, pag. 755, Antwerp 1982, K.H. Böckhoff (ed.).
- (24) Walter G., Käppeler F., Bao Z.Y., p.c. 1982.
- (25) Walter G., Beer H., Käppeler F., Penzhorn R.E., p.c. 1982.
- (26) Raman S., Fögelberg B., Harvey J.I., Macklin R.L., Stelson P.H., Schröder H., Kratz K.L. to appear in Phys. Rev. C 1983.
- (27) Akkermans J.M., Gruppelaar H., Reffo G., Phys.Rev. C 22, 73 (1980).
- (28) Gruppelaar H. contribution to this meeting.
- (29) Williams F.C., Jr., Nucl. Phys. A116, 231 (1971).

- (30) Costa C., "La conservazione del Momento angolare nei processi multistep compound". University of Bologna thesis. Relatore G.Reffo. Academic year 1980-81)
- (31) Reffo G., Herman M., Nuove Cimento Lett., 34, 261 (1982)
- (32) Becchetti F.D., Greenless G.W., Phys. Rev. 182, (1969) 1190.
- (33) Hermsdorf D., Meister A., Sassonoff S., Sceliger D., Scidel K., Shalvin P., Zentralinstitut für Kernforschung, Rossendorf Bei Dresden, ZfK-277(7) (1979).
- (34) Kamerdienev Y.L., report UCRL-51232 (1972).
- (35) D.Procopet et al. Soviet J.N.P. 34 (1981) 299.
- (36) A.Prince, G.Reffo, E.Sartori, "Spherical optical and Statistical Model Study" Report NEANDC-152 "A", INDC (NEA)4, 1983.
- (37) Gruppelaar H., p.c. 1983.

